Hindawi
Geofluids
Volume 2022, Article ID 5033940, 13 pages
https://doi.org/10.1155/2022/5033940

Research Article

Research on the Nonlinear Characteristics of Acoustic Emission and Damage Mechanism of Gassy Coal under Unloading Conditions

Jie Liu,[1,2,3] **Qiuping Li**,[1,2,3] **Ran Zhang**,[1,2,3] **Zaiquan Wang**,[4] **Shouqing Lu**,[1,2] **Zhanyou Sa**,[1,2] **and Hao Wang**[1,2]

[1]*Department of Safety Engineering, Qingdao University of Technology, Qingdao, Shandong 266520, China*
[2]*Key Lab of Industrial Fluid Energy Conservation and Pollution Control (Qingdao University of Technology), Ministry of Education, Qingdao, Shandong 266520, China*
[3]*Shandong Key Industry Field Accident Prevention Technology Research Center (Non-Ferrous Metallurgy), Qingdao, Shandong 266520, China*
[4]*School of Civil Engineering, Qingdao University of Technology, Qingdao, Shandong 266520, China*

Correspondence should be addressed to Jie Liu; liujie0805@qut.edu.cn

Received 26 January 2022; Accepted 7 March 2022; Published 25 March 2022

Academic Editor: Xuelong Li

Coal mining and production activities lead to static loading and unloading changes of coal stress in front of the working face, and the stress change process has a significant influence on the occurrence and development of coal-rock gas dynamic disasters. In this paper, the macroscopic failure characteristics, acoustic emission timing characteristics, and acoustic emission nonlinear characteristics of coal with different gas pressures under true triaxial loading and unloading conditions were experimentally studied. The results showed that the macroscopic failure form of coal with different gas pressures under unloading conditions was tensile-shear composite failure, and the crack structure was formed near the unloading surface. The fractal dimension D and multifractal parameter $\Delta\alpha$ of acoustic emission time series both could reflect the complexity of coal fracture process. With the increase of gas pressure, the fractal dimension D and multifractal parameter $\Delta\alpha$ decreased, which indicated that the greater the gas pressure, the lower the complexity of coal fracture process. Under different gas pressures, the dynamic change trends of multifractal parameter $\Delta\alpha$ were similar, taking the beginning of unloading as the dividing point, the change was roughly in the form of "W." When the stress state and failure form of coal body changed, the multifractal parameter $\Delta\alpha$ changed synchronously, indicating that the change of $\Delta\alpha$ could reflect the transformation process of failure mechanism of coal body under load to a certain extent, which was of great significance for clarifying the occurrence and development mechanism of coal-rock gas dynamic disasters and ensuring the safe production in underground coal mines.

1. Introduction

Coal occupies a dominant position in various energy resources in China, the largest coal producer and consumer in the world whose raw coal production increased from 1.08 to 4.07 billion tons from 1990 to 2021 [1, 2]. Therefore, the status of coal as the main energy source in China cannot be changed for a long time [3, 4]. Affected with increasing energy demand and mining intensity, the shallow coal resources in China are gradually depleted, and the mining is gradually transferred to the deep. Smaller stress perturbations may induce the occurrence of coal-rock gas dynamic disasters in deep mining, and the occurrence frequency of dynamic disasters increases gradually with more complex characteristics [5–9]. The safety of coal mining is greatly threatened affected by the production mode of coal mine

in China, which has put forward higher requirements for studying the occurrence mechanism of coal-rock gas dynamic disasters [10–13].

The stress disturbance could cause the coal body to deform and damage in the process of coal seam mining, which is directly related to the occurrence of coal-rock gas dynamic disasters [14, 15]. In the process of deformation and even destruction of coal bodies, the elastic energy accumulated inside them will be released to the outside in the form of elastic waves, and this phenomenon is called acoustic emission [16–19]. The variation of acoustic emission can reflect the law of elastic strain energy storage and consumption in coal body, which helps to clarify the process of coal body fracture under load, and many scholars have used acoustic emission technology to study the deformation and fracture process of coal rock. Su et al. studied the acoustic emission characteristics of coal samples during deformation and failure under different triaxial stress paths [20]. Ai et al. studied the spatial and temporal characteristics of acoustic emission in the process of coal-rock failure under triaxial conditions [21]. He et al. studied the acoustic emission characteristics of coal samples under triaxial cyclic loading-unloading conditions [22]. Kong et al. studied the variance and autocorrelation coefficients of acoustic emission time series under triaxial conditions by applying the critical slowing theory [23]. Aker et al. studied the acoustic emission and its moment tensor during triaxial fracture of rocks [24]. Du et al. investigated the change process of acoustic emission of gas-bearing coal and coal-rock combination during triaxial failure [25]. Yang et al. studied the acoustic emission spectrum characteristics of coal and sandstone fractured under the condition of triaxial confining pressure unloading [26]. Pan et al. investigated the statistical characteristics of acoustic emission of sandstone under the condition of triaxial confining pressure unloading [27].

The fracture process of coal rock is not continuous and is a nonlinear process. Therefore, the acoustic emission events generated in this process are also discrete and show obvious nonlinear characteristics. Since Mandelbrot proposed the fractal theory, a lot of achievements have been achieved by applying the theory to analyze the nonlinear characteristics of acoustic emission time series [28]. Yin et al. established and analyzed the fractal model of acoustic emission in the process of rock failure and considered that the continuous decrease of fractal dimension could characterize the instability failure of rock [29]. Kong and Li et al. calculated the correlation dimension of the acoustic emission event of coal rock under triaxial conditions and considered that the continuous decrease of the correlation dimension indicated the instability and failure of the coal samples [30, 31]. Guo et al. studied the fractal characteristics of acoustic emission in the process of uniaxial compression of shock-prone coal and believed that the sudden drop of fractal dimension after the peak value could be used as a precursor information for early warning of instability failure of coal samples [32]. Zhang et al. studied the multifractal characteristics of acoustic emission of gas-bearing coal under true triaxial loading-unloading conditions and concluded that the sudden increase of the multifractal parameter $\Delta\alpha$ can be used as a precursory feature to characterize the failure of coal samples [33].

Many scholars have used acoustic emission technology to study the process of coal-rock deformation and fracture, the focus of which is to use fractal theory to study the precursor information of coal-rock body fracture, which is of great help for the advance warning of coal-rock gas dynamic disaster. However, there are few reports on the relationship between the change of fractal parameters and the failure mechanism of coal. Therefore, on the basis of restoring the actual underground stress and gas conditions as much as possible, this paper designed true triaxial loading and unloading tests with different gas pressures to study the macroscopic failure characteristics, acoustic emission timing characteristics, and acoustic emission nonlinear characteristics of coal and further revealed the relationship between coal failure mechanism and acoustic emission nonlinear characteristics, which is of great significance for clarifying the occurrence and development mechanism of coal-rock gas dynamic disasters and ensuring safe production in coal mines.

2. Experiment Program

2.1. Experimental System. The true triaxial deformation and failure test system of gas-containing coal is shown in Figure 1, which consists of axial loading and unloading system (Figure 1(b)), confining pressure loading and unloading system (Figure 1(c)), sealing cavity (Figure 1(d)), gas seepage system (Figure 1(e)), and acoustic emission monitoring system (Figure 1(f)). The axial loading and unloading system adopts the electrohydraulic servo pressure testing machine controlled by microcomputer, which can realize load or displacement control and collect data and display them in real time. The confining pressure loading and unloading system was powered by two hydraulic systems to drive the cylinder. The working pressure of the hydraulic system was 0.48 MPa~28 MPa, and the working flow was 0~3.75 l/min. The acoustic emission system adopted the Express-8 8-channel acoustic emission equipment produced by American Physical Acoustics Company, which can collect the acoustic emission count, energy, amplitude, and other information in the process of coal-rock rupture under load and can simultaneously collect the acoustic emission signal.

2.2. Sample Preparation and Experimental Scheme. In order to restore the original environment in which the coal seam was located as much as possible, complete large coal samples were taken from the retrieved workings as test coal samples for the true triaxial loading and unloading test. According to the test requirements of the International Society of Rock Mechanics, the large coal samples were cut into 100 mm × 100 mm × 100 mm cubic raw coal samples in the laboratory, and the surface of the sample was polished by a grinding machine to make the unevenness of the surface of the specimen less than 0.05 mm. And the ultrasonic testing was carried out on each surface of the sample to obtain the wave velocity values of each face, and the coal samples with small error of wave velocity values of each surface were selected as test coal samples, so as to avoid the occurrence of large test error as much as possible. In order to better

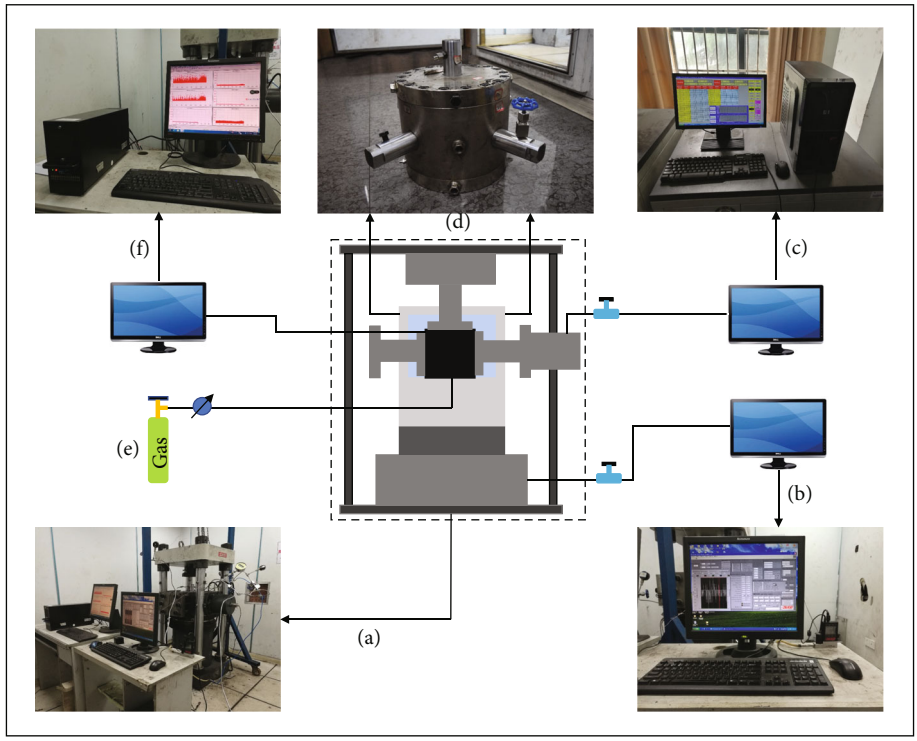

Figure 1: Diagram of experimental system.

ensure the adsorption effect and sealing effect of the gas, silica gel was applied on the surface of the sample to be condensed, and then, it was sealed in the heat shrink tube as shown in Figure 2. Finally, the prepared coal samples were numbered and stored in a constant temperature incubator.

It was necessary to carry out conventional triaxial loading experiments to obtain the strength of coal samples at different gas pressure. 80% of the strength is taken as the initial unloading stress in the true triaxial loading and unloading experiments. Three coal samples were selected from conventional triaxial test and true triaxial loading and unloading experiment under different gas pressures, and the specific test conditions are shown in Table 1. The specific process of conventional triaxial loading test and true triaxial unloading test is as follows:

(1) Conventional triaxial loading experiment: firstly, the coal sample was put into the experiment chamber for air tightness detection, and then, a vacuum pump was used to evacuate for 24 hours. Secondly, after the preparation, the axial pressure and confining pressure were gradually applied to the design value of 19 MPa according to the loading method of hydrostatic pressure, and then, the gas was, respectively, charged with 0 MPa, 0.2 MPa, 0.5 MPa, and 0.8 MPa, and the gas was adsorbed for 24 hours. After the gas adsorption equilibrium, the axial load was continuously applied at the loading speed of 500 N/s until the coal body was destroyed, and the load and displacement data were collected at the same time. The stress path diagram of conventional triaxial loading and unloading test is shown in Figure 3(a)

(2) True triaxial loading and unloading experiment: the test preparation was the same as (1). After the gas adsorption under different conditions was balanced, the axial load was loaded at the speed of 500 N/s to 80% of the strength, and then, the axial load remained unchanged. Next, the horizontal stress was unloaded at the speed of 0.005 MPa/s and 0.02 MPa/s, respectively, and the test was stopped after the coal body rupture. The stress path diagram of true triaxial loading and unloading test is shown in Figure 3(b)

3. Experimental Results

3.1. Macroscopic Failure Characteristics of Coal Samples. Due to the large number of test groups, only one group of samples under each test condition was selected for analysis in this paper. Figure 4 shows the macroscopic failure characteristics of gas-containing coal under different gas pressure conditions, and the surface perpendicular to the direction of the minimum principal stress was defined as the unloading surface in the paper. On the whole, the macroscopic failure forms of coal under different gas pressures were all composite tension-shear failures. On the plane perpendicular to the minimum principal stress, cracks in the gas-bearing coal body gradually developed to form the main fracture surface. The shear failure mostly occurred at a position far from the unloading surface, and as the distance from the unloading surface got closer and closer, the failure of the coal sample gradually transitioned to tension, and more splitting tension was formed near the unloading surface. This was because after the horizontal stress began to be

Figure 2: Experimental samples.

Table 1: Experimental condition.

Experimental name	Number	Confining pressure σ_2, σ_3 (MPa)	Gas pressure (MPa)	σ_2 unloading rate (MPa/s)	σ_3 unloading rate (MPa/s)
Conventional triaxial-0	1, 2, 3	19	0	—	—
Conventional triaxial-0.2	4, 5, 6	19	0.2	—	—
Conventional triaxial-0.5	7, 8, 9	19	0.5	—	—
Conventional triaxial-0.8	10, 11, 12	19	0.8	—	—
True triaxial loading and unloading experiment-0	1, 2, 3	19	0	0.005	0.02
True triaxial loading and unloading experiment-0.2	4, 5, 6	19	0.2	0.005	0.02
True triaxial loading and unloading experiment-0.5	7, 8, 9	19	0.5	0.005	0.02
True triaxial loading and unloading experiment-0.8	10, 11, 12	19	0.8	0.005	0.02

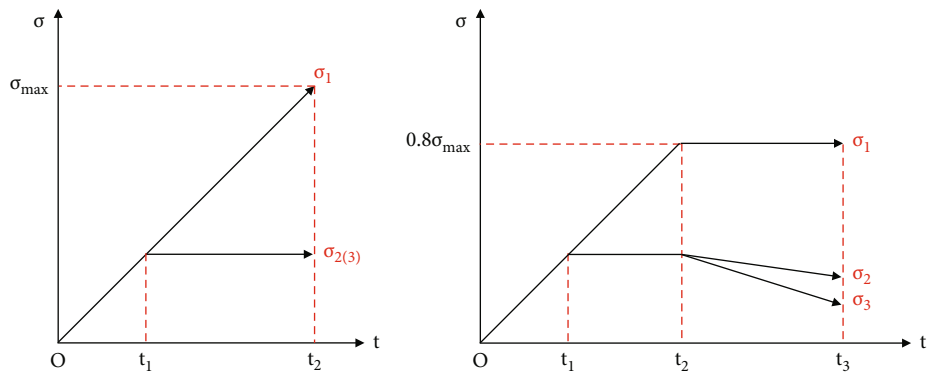

(a) Conventional triaxial loading test (b) True triaxial loading and unloading experiment

Figure 3: Stress path map.

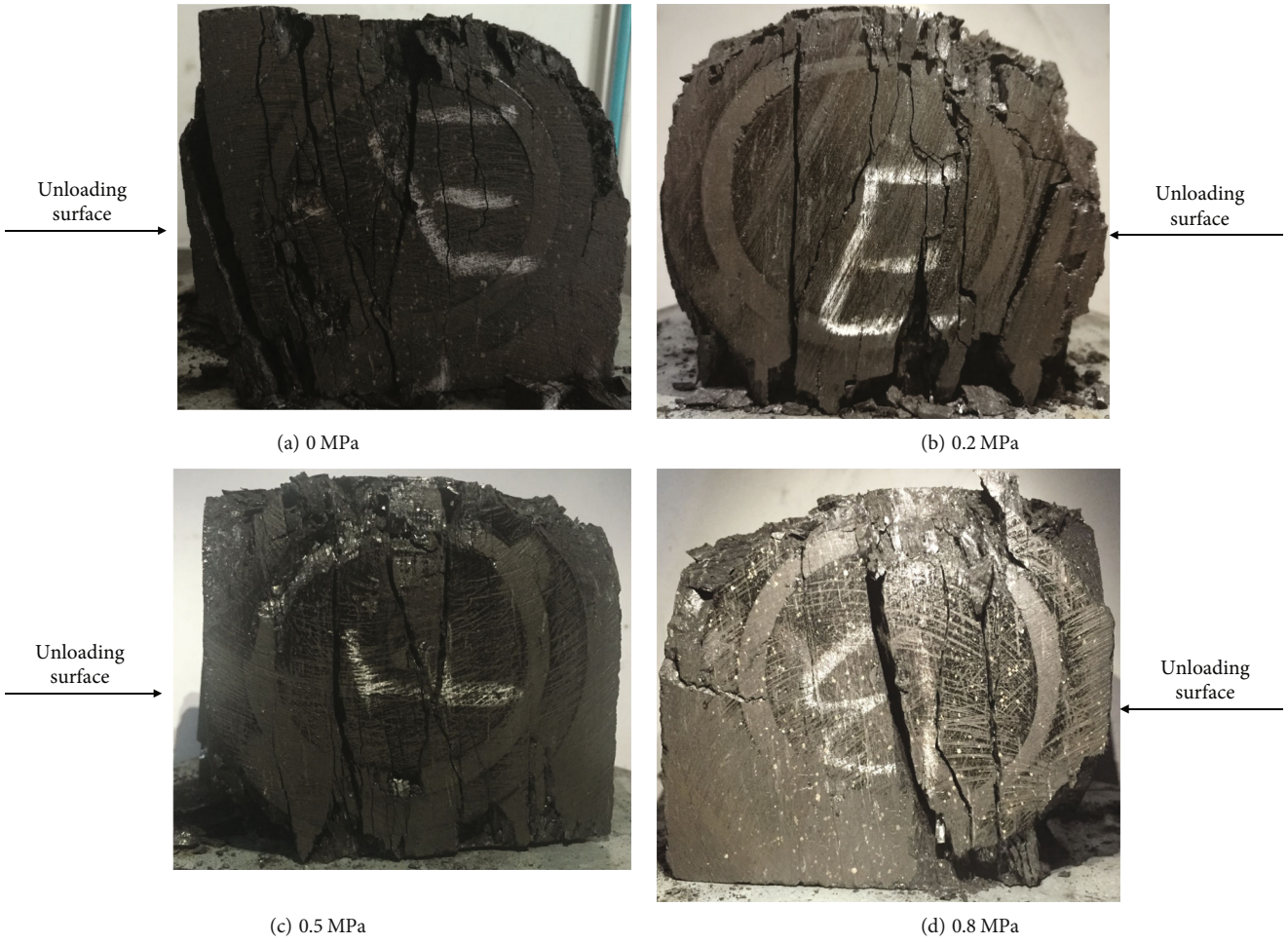

Figure 4: Failure modes of coal samples under different gas pressures.

unloaded to a lower level, the stress state of the coal body could be approximately regarded as vertical unidirectional stress, and the coal sample was mainly fractured by tension crack under this stress state. Therefore, the splitting tensile cracks would be formed near the unloading surface, which showed that the failure near the unloading surface was mostly in the form of splitting into plate and plate bending.

Although the overall failure of the coal samples at different gas pressure was in the form of tension shear, the development degree of cracks was obviously different. With the increase of gas pressure, the development degree of splitting tensile cracks near the unloading surface gradually decreased. When the gas pressure was low, a large number of splitting tensile cracks appeared near the unloading surface, and the larger the gas pressure was, the less the number of splitting tensile cracks was. The reason was that when the gas pressure was low, the weakening effect of gas on the bearing capacity of coal was small. After the minimum principal stress began to unload, the coal sample would undergo a relatively long unloading process before the strength failure occurred. In this process, tensile failure mainly occurred, and splitting and tensile cracks developed in large quantities; when the gas pressure was large, the bearing capacity of the coal sample was greatly weakened, and the coal sample lost its bearing capacity after a short unloading time, resulting in less tensile cracks.

3.2. Temporal Characteristics of Acoustic Emission. The acoustic emission signal is generated by the fracture of the coal body, and it can reflect the failure process of gas-containing coal. This section analyzed the temporal characteristics of acoustic emission during the loading process of coal samples. Due to the gas-bearing coal presenting the fracture form of tension-shear composite under the true triaxial loading and unloading conditions, the generalized shear stress it underwent could be expressed by the difference between the axial stress σ_1 and the two horizontal stresses σ_2 [3]; when the stress difference ($\sigma_1 - \sigma_2$ [3]) began to decrease, it meant that the coal body gradually lost its bearing capacity. Therefore, the stress difference ($\sigma_1 - \sigma_2$ [3]) could more clearly indicate the stress of gas-bearing coal under true triaxial loading and unloading. Figure 5 shows the stress difference-acoustic emission test results of coal samples under different gas pressures. And it can be seen from the test results that the overall change law of acoustic

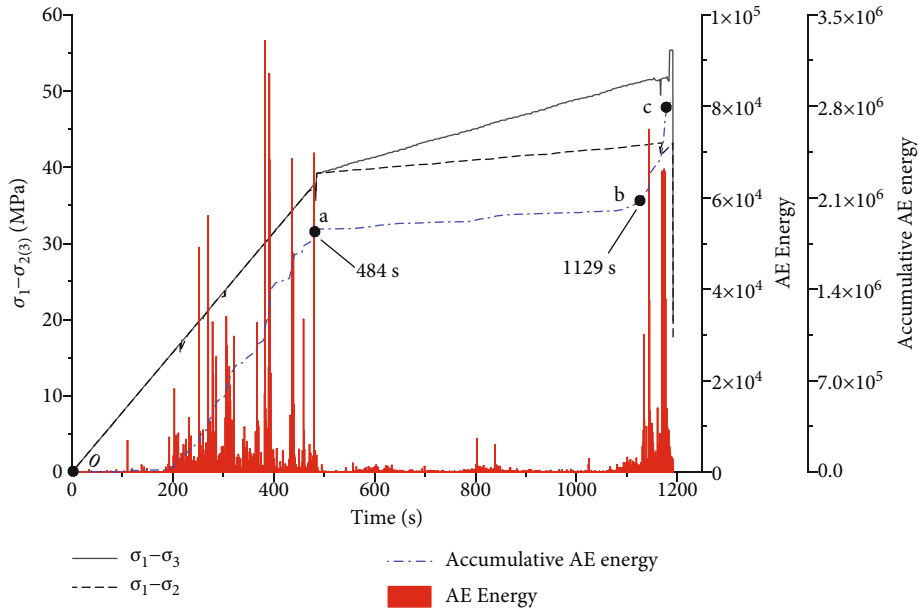

(a) Gas pressure 0 MPa

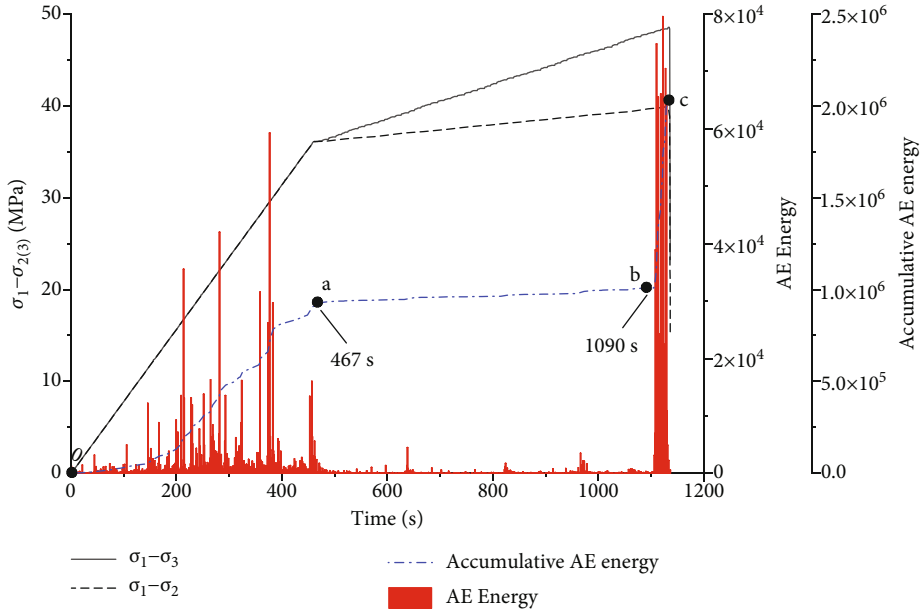

(b) Gas pressure 0.2 MPa

Figure 5: Continued.

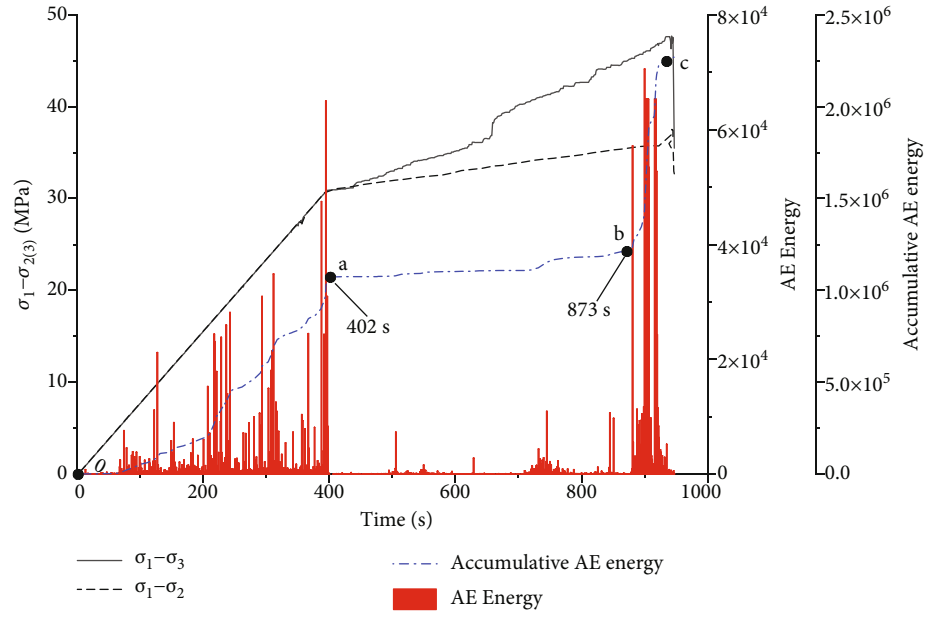

(c) Gas pressure 0.5 MPa

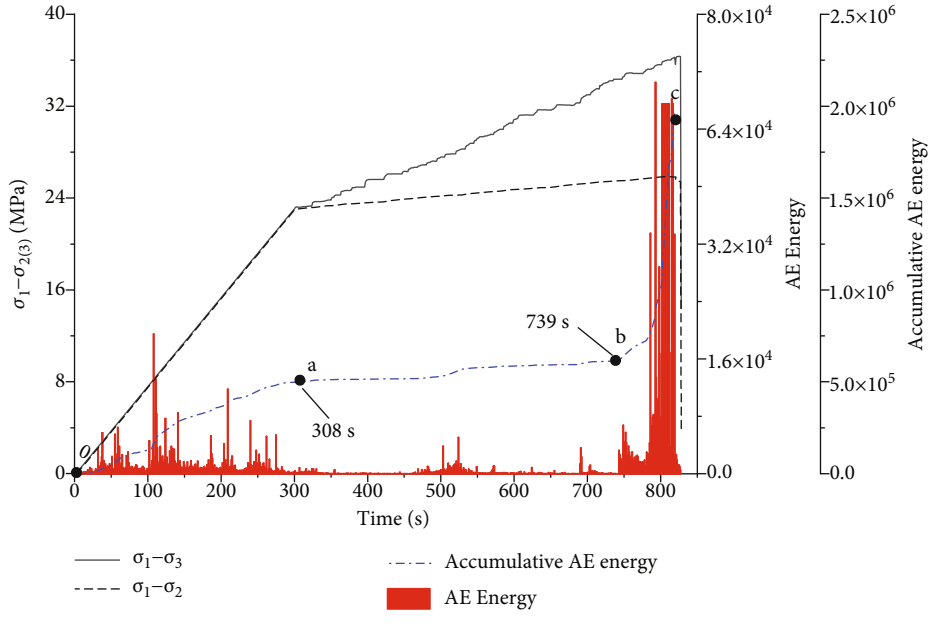

(d) Gas pressure 0.8 MPa

Figure 5: Time series characteristics of acoustic emission under different gas pressures.

emission time series under different gas pressure conditions shows a similar trend. Based on the accumulated energy of acoustic emission, the process of acoustic emission change can be roughly divided into three stages:

(1) Continuous growth stage (*oa*): at this stage, the acoustic emission energy signal was relatively active, and with the continuous increase of the axial stress, the acoustic emission energy increased continuously, and the accumulated acoustic emission energy showed a trend of continuous growth. This was because the external energy was continuously input into the coal body, prompting the extension and expansion of the cracks in the coal body and generating a large number of acoustic emission signals. At the same time, under the action of gas, the primary cracks in the coal sample were further developed, and the expansion and extension of many cracks were superimposed on each other, which made the acoustic emission events gradually active. In addition, since the axial stress had been increased to 80% of the strength of the sample at

this stage, the cracks inside the sample would extend and penetrate to a certain extent, resulting in local rupture and a large acoustic emission signal

(2) Calm phase (*ab*): in this stage, the axial stress remained constant, the two horizontal stress began to unload, and the acoustic emission signal decreased significantly and tended to be calm, showing obvious paroxysm, and the accumulated energy of acoustic emission remained basically unchanged. This was because the external energy was no longer input, and only when the confining pressure decreased to a certain value and the axial stress exceeded the limit of crack extension strength under this confining pressure, the cracks in the coal body continued to expand, resulting in acoustic emission signals. Therefore, the acoustic emission signals were not active in the calm phase. Under different gas pressure conditions, the duration of the calm phase was different. It could be seen from Figure 5 that when the gas pressure was 0 MPa, 0.2 MPa, 0.5 MPa, and 0.8 MPa, the calm phase lasted for 645 s, 622 s, 471 s, and 431 s, respectively. This was because the gas changed the internal structure of the coal body, which reduced the energy storage threshold of the coal body. The greater the gas pressure, the weaker the ability of the coal sample to resist deformation and failure, and the shorter the duration of the calm stage

(3) Accelerated growth stage (*bc*): when the stress difference reached the strength limit of the sample, the acoustic emission signal increased intensively, the acoustic emission energy value increased rapidly, and the corresponding acoustic emission cumulative energy accelerated. During this stage, the newly generated cracks expanded and interpenetrated with the original cracks in the coal sample, resulting in the formation of macroscopic fractures until the coal sample completely lost its load-bearing capacity. Due to the large amount of elastic energy accumulated in the early stage of loading-unloading, the release of the internal accumulated elastic energy led to the emergence and penetration of new cracks at this stage. At the same time, the formation of new cracks accelerated the desorption of gas inside the coal sample, which further changed the internal structure of the coal sample; all of which led to the intensive increase of acoustic emission signal in this stage

4. Discussion

In order to further clarify the failure mechanism of gas-bearing coal under true triaxial loading and unloading conditions, the *R*/*S* statistical characteristics and multifractal characteristics of acoustic emission time series during fracture process were analyzed.

4.1. R/S Statistical Characteristics of Acoustic Emission Time Series. The theory of the *R*/*S* statistical analysis method, proposed by Hurst in 1956, was supplemented and improved by Mandelbrot and it gradually developed into the fractal theory for studying time series. Since then, the theory has been widely used in rock mechanics and earth science [34].

The time series of acoustic emission signals in the deformation and fracture process of gas-bearing coal under unloading conditions are recorded as follows [34].

$$\{x(t), t = 1, 2, \cdots, N\}. \tag{1}$$

It is divided into N subsequences with length k, and the mean values of each subsequence are calculated, respectively:

$$\langle X\rangle_k = \frac{1}{k}\sum_{t=1}^{k} x(t). \tag{2}$$

Accumulated deviation:

$$X(n,k) = \sum_{i=1}^{n}\left(x(i) - \langle X\rangle_k\right), \quad 1 \le n \le k. \tag{3}$$

Extreme difference:

$$R(k) = \max_{1\le n\le k} X(n,k) - \min_{1\le n\le k} X(n,k). \tag{4}$$

Standard deviation:

$$S(k) = \sqrt{\frac{1}{k}\sum_{i=1}^{k}\left[x(t) - \langle X\rangle_k\right]^2}. \tag{5}$$

From *R*/*S* statistical analysis,

$$\frac{R(k)}{S(k)} \sim (k)^H. \tag{6}$$

Among them, H is the Hurst index.

By transforming Equation (6), we can obtain

$$H = \frac{d\log\left(R(k)/S(k)\right)}{d\log(k)}. \tag{7}$$

The tangent value of the relationship curve between $d\log(R(k)/S(k))$ and $d\log(k)$ was the Hurst index H of the analyzed time series.

In the *R*/*S* statistical analysis method, when $0 < H < 0.5$, it meant that the analyzed time series showed a decreasing trend over time, i.e., they had negative correlation; when $H = 0.5$, it indicated that the analyzed time series did not affect each other on each scale; when $0.5 < H < 1$, it meant that the analyzed time series showed an increasing trend over time, i.e., they had positive correlation. According to the characteristics of *R*/*S* statistical analysis method, the Hurst index value could be used to study the internal trend characteristics of acoustic emission time series in the deformation and

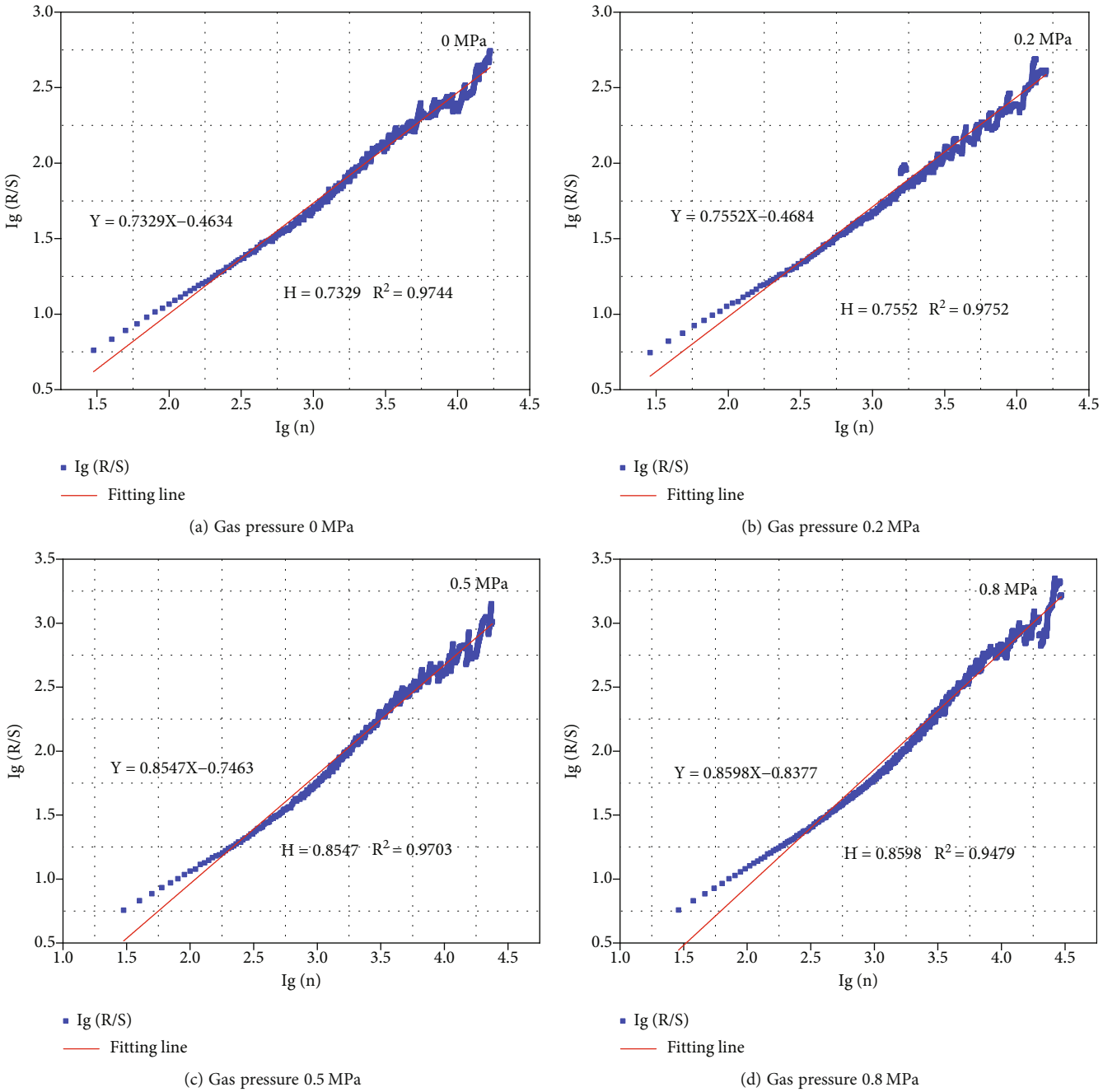

(a) Gas pressure 0 MPa

(b) Gas pressure 0.2 MPa

(c) Gas pressure 0.5 MPa

(d) Gas pressure 0.8 MPa

Figure 6: *R*/*S* statistical rule of acoustic emission signal.

fracture process of gas-bearing coal. Therefore, the acoustic emission time series obtained from the test were calculated as shown in Figure 6.

Figure 6 shows the relationship between the acoustic emission signal $d \log (R(k)/S(k))$ and $d \log (k)$ under different gas pressures. The tangent of the curve was calculated and the Hurst index was obtained at the same time, which showed that the acoustic emission signal under different gas pressures had strong *R*/*S* statistical law and the Hurst index was greater than 0.5, and the correlation coefficient *R*2 was greater than 0.9, indicating that the acoustic emission signal showed an overall trend of enhancement with the passage of time and the increasing of stress difference, and the acoustic emission signal had a positive correlation with time. At the same time, with the increase of gas pressure, the Hurst index also showed an increasing trend, and its positive correlation was stronger; this was because gas would change the internal structure of the coal body, thereby weakening the bearing capacity of the coal body. And the larger the gas pressure was, the worse the bearing capacity of coal body was, the more severe the fracture of the sample was, and the stronger the acoustic emission signal in the process of damage and failure was, which was manifested in the increase of Hurst index.

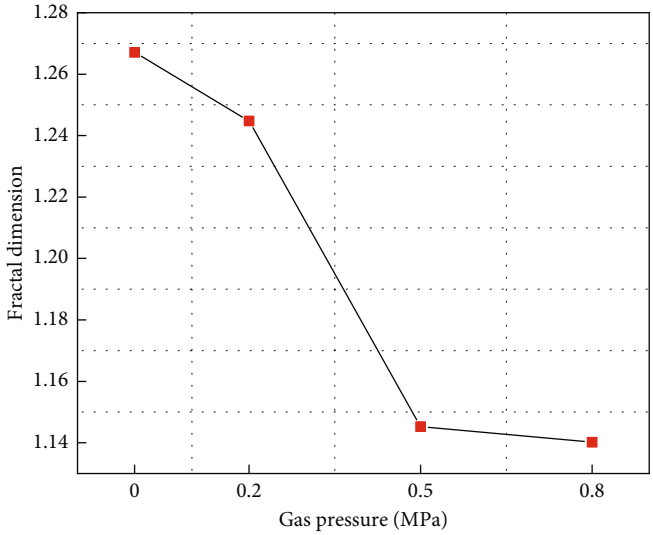

Figure 7: The simple fractal dimension changes.

There is a relationship between Hurst index H and simple fractal dimension D [31].

$$D = 2 - H. \tag{8}$$

Fractal dimension D value was often used to analyze the irregularity and complexity of specific time series. In this paper, since the acoustic emission signal could reflect the degree of deformation and rupture of coal rock, the fractal dimension D of the acoustic emission time series could be used to analyze the complexity of the deformation and rupture process of the coal sample under load. The larger value of D indicated that the deformation and fracture process was more complex; the smaller value of D indicated that the coal rock deformation and fracture process was relatively simple and more regular [28]. Figure 7 shows the change of fractal dimension of acoustic emission time series under different gas pressures. It could be seen that the simple fractal dimension showed a decreasing trend with the continuous increase of gas pressure, and the fractal dimension was the largest when the gas pressure was 0 MPa and the smallest at gas pressure 0.8 MPa, which indicated that the complexity of the deformation and rupture process of coal samples decreased with the larger gas pressure, and its destruction presented a certain regularity.

The change rule of fractal dimension had a certain correlation with the macroscopic fracture morphology of coal samples; the macroscopic fracture of the sample all showed the form of tension-shear composite fracture. When the gas pressure was small, the tension crack in coal samples was more, resulting in the complicated destruction process of coal body, which showed that the fractal dimension was large. However, with the increasing of gas pressure, the bearing capacity of coal body gradually decreased, and the coal sample failure occurred in a relatively short time, and the number of cleavage cracks was relatively small, especially at the gas pressure of 0.8 MPa. Thus, the fractal dimension decreased when the gas pressure was higher, indicating that the failure process of coal sample was relatively simple and had a certain regularity.

4.2. Multifractal Characteristics of Acoustic Emission Signals. Hurst index and fractal dimension D could reflect the change trend of acoustic emission time series and the complexity of coal deformation and fracture process as a whole, while the deformation and fracture of coal rock under load was a nonlinear change process. And the closure, initiation, extension, and penetration of internal cracks were not continuous, and the acoustic emission signals were discrete and nonlinear. The deconstruction analysis of the change process of acoustic emission of gas-bearing coal under unloading conditions by using multiple fractal calculation method could help reveal the dynamic change process of deformation and fracture.

In this paper, the box dimension method was used to calculate the multifractal features of the acoustic emission time series [35–39]. Firstly, a partition function was defined, that is, the statistical moment:

$$X_q(\varepsilon) \equiv \sum P_i(\varepsilon)^q \sim \varepsilon^{\tau(q)}, \tag{9}$$

where $\tau(q)$ is the mass index, $-\infty < q < +\infty$.

When there is a power exponential relationship between the defined collocation function and the division scale ε, i.e., Equation (9) holds, the value of $\tau(q)$ can be calculated from the slope of the double logarithmic curve $\ln Xq(\varepsilon) - \ln \varepsilon$, i.e.,

$$\tau(q) = \lim_{\varepsilon \longrightarrow 0} \frac{\ln X_q(\varepsilon)}{\ln \varepsilon}. \tag{10}$$

The Legendre transformation of $\tau(q) - q$

$$\alpha = \frac{d(\tau(q))}{dq} = \frac{d}{dq}\left(\lim_{\varepsilon \longrightarrow 0} \frac{\ln X_q(\varepsilon)}{\ln \varepsilon}\right), \tag{11}$$

$$f(\alpha) = \alpha q - \tau(q). \tag{12}$$

The $\alpha - f(\alpha)$ curve composed of α and $f(\alpha)$ is the multifractal spectrum of the calculated acoustic emission time series, which can reflect the properties of the random distribution within the AE time series [30–34]. α represents the signal subset in the acoustic emission time series, where α_{max} represents the large signal corresponding to the subset and α_{min} represents the small signal corresponding to the subset. Therefore, the multifractal spectrum width $\Delta\alpha = \alpha_{max} - \alpha_{min}$ can reflect the difference between signals, and the greater the $\Delta\alpha$, the more the difference between them. Large-scale fracture of gassy coal generates acoustic emission signals with high energy, and small-scale fracture of gassy coal generates acoustic emission signals with low energy. $\Delta\alpha$ could distinguish the acoustic emission signals with high or low energy, and $f(\alpha)$ reflect the number difference between high and low energy, so $\Delta\alpha$ combined with $f(\alpha)$ reflect the deformation and fracture process of gassy coal.

Figure 8 shows the multifractal spectra of the acoustic emission time series under different gas pressures. It can be seen that the multifractal spectra of different gas pressures under unloading conditions are all in the shape of right hook, which indicated that the small signal of acoustic emission dominated the whole process of coal sample rupture under load. In addition, as the gas pressure increased, $\Delta\alpha$ of the acoustic emission time series decreased gradually, indicating that the greater the gas pressure under unloading conditions, the smaller the difference between the large and small signals in the process of coal sample rupture under load, the lower the complexity of the coal sample rupture process, which was the same as the change trend of fractal dimension D.

In order to clarify the dynamic change process of the coal sample under load and to understand the failure mechanism of the coal sample under the unloading condition as much as possible, the variation law of $\Delta\alpha$ under different stress difference levels during the test was studied. We studied the variation law of $\Delta\alpha$ under different stress difference levels in the test process. Figure 9 shows the variation law of $\Delta\alpha$ under different stress difference levels. Under different gas pressures, the overall variation law of $\Delta\alpha$ was consistent with the increase of the stress difference level. With the beginning of unloading as the dividing point, $\Delta\alpha$ decreased continuously before the start of unloading and $\Delta\alpha$ fluctuated after the beginning of unloading; when the stress difference level was close to the rupture load, $\Delta\alpha$ increased sharply until complete rupture, roughly showing a "W"-type change.

Before the start of unloading, the coal sample was in the state of triaxial loading, the failure at this time was mainly shear failure, and the $\Delta\alpha$ value always developed in a decreasing trend. When the stress difference was small, the sample was in the compaction stage. At this time, a large number of micro cracks were closed and developed under

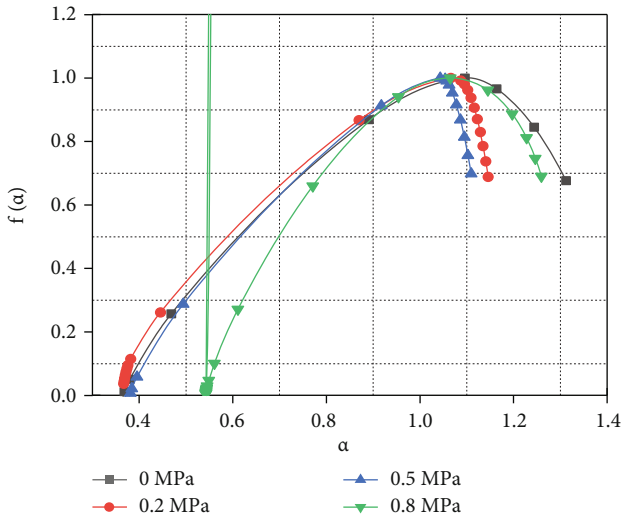

Figure 8: Multifractal spectra of different gas pressure.

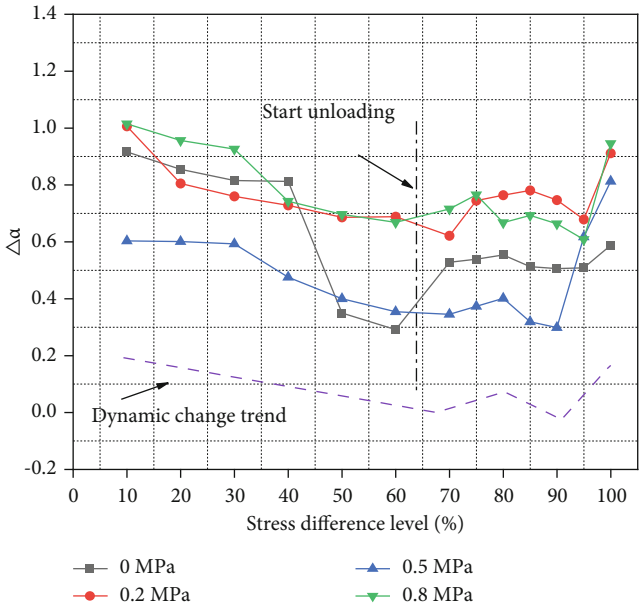

Figure 9: Different stress levels $\Delta\alpha$.

the action of external force, the development of cracks was more complicated, and the $\Delta\alpha$ value was relatively large. Then, with the increase of axial load, the sample gradually entered the elastic deformation stage. At the same time, the development of cracks was dominated by friction slip, the complexity of coal fracture was reduced, and the $\Delta\alpha$ value was gradually reduced. When the unloading started, the stress state of the coal sample changed. Due to the reduction of the horizontal stress, the stress state of coal samples gradually transited from three-way loading to vertical uniaxial loading. And in the case of uniaxial loading, the failure of the coal sample was mainly splitting and tensile failure. Therefore, under the transition stress state from three-way loading to vertical uniaxial loading, the failure form of the coal sample began to change. On the basis of the development of shear cracks dominated by friction and slip in the

early stage, the development of splitting tensile cracks gradually increased, the fracture process of coal samples began to become complicated, and the $\Delta\alpha$ value began to increase and fluctuate. When the stress difference was close to the critical failure load, the cracks in the coal body began to extend and penetrate, and the fracture network gradually developed into the main fracture surface. At this time, the complexity of the coal sample rupture process was further enhanced, and the $\Delta\alpha$ value increased rapidly until the coal sample was completely ruptured. Therefore, the dynamic change of multifractal parameter $\Delta\alpha$ could reflect the fracture process of coal body and to a certain extent could represent the failure mechanism of coal body under load, which was of great significance for understanding the occurrence and development mechanism of coal rock gas dynamic disasters and improving the accuracy of early warning.

5. Conclusions

(1) Under unloading conditions, the macroscopic failure forms of coal with different gas pressures were all composite tension-shear failures. On the plane perpendicular to the minimum principal stress, the cracks in the gas-bearing coal body gradually developed to form the main failure surface. The shear failure mostly occurred at a position far from the unloading surface, and as the distance from the unloading surface got closer and closer, the failure of the coal sample gradually transitioned to tension, and more splitting tension was formed near the unloading surface

(2) The acoustic emission signal had a strong R/S statistical law under different gas pressures and the Hurst indexes were all greater than 0.5, which indicated that the acoustic emission signal showed an overall increasing trend with the passage of time and the increasing stress difference. And there was a positive correlation between the acoustic emission signal and time. With the increase of gas pressure, Hurst index also showed an increasing trend, and its positive correlation was enhanced

(3) Both the fractal dimension D and the multifractal parameter $\Delta\alpha$ could reflect the complexity of the coal sample fracturing process. With the increase of the gas pressure, the fractal dimension D and the multifractal parameter $\Delta\alpha$ decreased, which meant that the larger the gas pressure was, the higher the less complexity of the coal sample rupture process was

(4) Under different gas pressures, the overall variation of $\Delta\alpha$ was consistent with the increase of the stress difference level. Taking the start of unloading as the dividing point, $\Delta\alpha$ decreased continuously before the start of unloading, and $\Delta\alpha$ showed a fluctuating change after the start of unloading, and when the stress difference level was close to the rupture load, $\Delta\alpha$ increased sharply until complete rupture, roughly showing a "W" shape change. The dynamic change of the multifractal parameter $\Delta\alpha$ could reflect the fracture process of the coal mass, and to a certain extent, it could represent the failure mechanism of the coal mass under load, which was useful for understanding the occurrence and development mechanism of coal-rock gas dynamic disasters and improving the accuracy of early warning

Data Availability

The experimental and calculated data used to support the findings of this study are included within the article.

Conflicts of Interest

The authors declare no competing financial interests or personal relationships that could have appeared to influence the work in this paper.

Acknowledgments

This work was supported by the National Natural Science Foundation of China (51974169), Natural Science Foundation of Shandong Province (ZR2020QE124), and China Postdoctoral Science Foundation (2018M642632 and 2019M652346).

References

[1] *Energy Production in December of 2021*http://www.stats.gov.cn/english/PressRelease/202201/t20220118_1826644.html.

[2] H. Jiang and Y. Luo, "Development of a roof bolter drilling control process to reduce the generation of respirable dust," *Int J Coal Sci Technol.*, vol. 8, no. 2, pp. 199–204, 2021.

[3] Statistical Communiqué of the People's Republic of China on the 2020, *National Economic and Social Development*http://www.stats.gov.cn/english/PressRelease/202102/t20210228_1814177.html.

[4] S. Lu, C. Wang, M. Li et al., "Gas time-dependent diffusion in pores of deformed coal particles: model development and analysis," *Fuel*, vol. 295, article 120566, 2021.

[5] M. He, H. Xie, S. Peng, and Y. Jiang, "Study on rock mechanics in deep mining engineering," *Chinese Journal of Rock Mechanics and Engineering.*, vol. 24, no. 16, pp. 2803–2813, 2005.

[6] X. He and L. Song, "Status and future tasks of coal mining safety in China," *Safety Science*, vol. 50, no. 4, pp. 894–898, 2012.

[7] S. Lu, C. Wang, W. Wang, M. Li, and D. Zhang, "Analysis on the shape and impact pressure of the high-pressure water jet during the hydraulic flushing cavity technique," *Geofluids*, vol. 2021, Article ID 7496540, 2021.

[8] S. Lu, C. Wang, Q. Liu et al., "Numerical assessment of the energy instability of gas outburst of deformed and normal coal combinations during mining," *Process Safety and Environmental Protection*, vol. 132, pp. 351–366, 2019.

[9] P. Zhao, J. Wang, S. Li et al., "Effects of recovery ratio on the fracture evolution of the overburden pressure-relief gas migration channel for a fully mechanized working face," *Natural Resources Research*, pp. 1–16, 2022.

[10] J. Liu, R. Zhang, D. Song, and Z. Wang, "Experimental investigation on occurrence of gassy coal extrusion in coalmine," *Safety Science*, vol. 113, pp. 362–371, 2019.

[11] R. Zhang, J. Liu, Z. Sa, Z. Wang, S. Lu, and Z. Lv, "Fractal characteristics of acoustic emission of gas-bearing coal subjected to true triaxial loading," *Measurement*, vol. 169, article 108349, 2021.

[12] S. Lu, Y. Zhang, Z. Sa, S. Si, L. Shu, and L. Wang, "Damage-induced permeability model of coal and its application to gas predrainage in combination of soft coal and hard coal," *Energy Sci Eng.*, vol. 7, no. 4, pp. 1352–1367, 2019.

[13] C. Wang, *Research of Rockburst Risk Comprehensive Evaluation Method Based on Unascertained Measurement Model and Application*, Published online, 2011.

[14] H. Jiang, Y. Luo, and J. Yang, "The mechanics of bolt drilling and theoretical analysis of drilling parameter effects on respirable dust generation," *Journal of Occupational and Environmental Hygiene*, vol. 15, no. 9, pp. 700–713, 2018.

[15] S. Liu, X. Li, D. Wang, and D. Zhang, "Experimental study on temperature response of different ranks of coal to liquid nitrogen soaking," *Natural Resources Research*, vol. 30, no. 2, pp. 1467–1480, 2021.

[16] M. C. He, J. L. Miao, and J. L. Feng, "Rock burst process of limestone and its acoustic emission characteristics under true-triaxial unloading conditions," *International Journal of Rock Mechanics and Mining Sciences*, vol. 47, no. 2, pp. 286–298, 2010.

[17] S. J. D. Cox and P. G. Meredith, "Microcrack formation and material softening in rock measured by monitoring acoustic emissions," *International Journal of Rock Mechanics and Mining Sciences & Geomechanics Abstracts.*, vol. 30, no. 1, pp. 11–24, 1993.

[18] D. A. Lockner, J. D. Byerlee, V. Kuksenko, A. Ponomarev, and A. Sidorin, "Quasi-static fault growth and shear fracture energy in granite," *Nature*, vol. 350, no. 6313, 1991.

[19] S. Lu, Y. Zhang, Z. Sa, and S. Si, "Evaluation of the effect of adsorbed gas and free gas on mechanical properties of coal," *Environment and Earth Science*, vol. 78, no. 6, 2019.

[20] C. Su, B. Gao, H. Nan, and X. Li, "Experimental study on acoustic emission characteristics during deformation and failure processes of coal samples under different stress paths," *Yanshilixue Yu Gongcheng Xuebao/Chinese Journal of Rock Mechanics and Engineering.*, vol. 28, no. 4, pp. 757–766, 2009.

[21] T. Ai, R. Zhang, J. F. Liu, X. P. Zhao, and L. Ren, "Space-time evolution rules of acoustic emission locations under triaxial compression," *Meitan Xuebao/Journal of the China Coal Society.*, vol. 36, no. 12, pp. 2048–2057, 2011.

[22] J. He, J. N. Pan, and A. H. Wang, "Acoustic emission characteristics of coal specimen under triaxial cyclic loading and unloading," *Meitan Xuebao/Journal of the China Coal Society.*, vol. 39, no. 1, pp. 84–90, 2014.

[23] X. Kong, E. Wang, S. Hu et al., "Critical slowing down on acoustic emission characteristics of coal containing methane," *Journal of Natural Gas Science and Engineering.*, vol. 24, pp. 156–165, 2015.

[24] E. Aker, D. Kühn, V. Vavryčuk, M. Soldal, and V. Oye, "Experimental investigation of acoustic emissions and their moment tensors in rock during failure," *International Journal of Rock Mechanics and Mining Sciences.*, vol. 70, pp. 286–295, 2014.

[25] F. Du, K. Wang, G. Wang, Y. Jiang, C. Xin, and X. Zhang, "Investigation of the acoustic emission characteristics during deformation and failure of gas-bearing coal-rock combined bodies," *Journal of Loss Prevention in the Process Industries*, vol. 55, pp. 253–266, 2018.

[26] Y. Yang, D. Ma, and Y. Zhou, "Experimental research on spectrum signature eigen of acoustic emission of coal and sandstone damage under triaxial unloading confining pressure," *Caikuang yu Anquan Gongcheng Xuebao/Journal of Mining and Safety Engineering.*, vol. 36, no. 5, pp. 1002–1008, 2019.

[27] X. Pan, J. Chen, and D. Jiang, "Statistical characteristics of sandstone acoustic emission under triaxial unloading confining pressure," *Meitan Xuebao/Journal of the China Coal Society.*, vol. 43, no. 10, pp. 2750–2757, 2018.

[28] B. B. Mandelbrot, P. DannE, and A. J. Paullay, "Fractal character of fracture surfaces of metals," *Nature*, vol. 308, no. 5961, pp. 721-722, 1984.

[29] X. G. Yin, S. L. Li, and H. Y. Tang, "Study on strength fractal features of acoustic emission in process of rock failure," *Yanshilixue Yu Gongcheng Xuebao/Chinese Journal of Rock Mechanics and Engineering*, vol. 24, no. 19, pp. 3512–3516, 2005.

[30] X. Kong, E. Wang, S. Hu, R. Shen, X. Li, and T. Zhan, "Fractal characteristics and acoustic emission of coal containing methane in triaxial compression failure," *Journal of Applied Geophysics*, vol. 124, pp. 139–147, 2016.

[31] D. Li, E. Wang, and X. Kong, "Fractal characteristics of acoustic emissions from coal under multi-stage true-triaxial compression," *Journal of Geophysics and Engineering*, vol. 15, no. 5, pp. 2021–2032, 2018.

[32] H. Guo, D. Song, X. He, Q. Lou, and L. Qiu, "Fractal characteristics of acoustic emission in different damage degrees of impact coal," *Coal Science and Technology*, vol. 49, no. 9, pp. 38–46, 2021.

[33] R. Zhang, J. Liu, Z. Sa, Z. Wang, S. Lu, and C. Wang, "Experimental investigation on multi-fractal characteristics of acoustic emission of coal samples subjected to true triaxial loading-unloading," *Fractals*, vol. 28, no. 5, 2020.

[34] Y. Y. Li, K. L. Yin, and W. M. Cheng, "Application of R/S method in forecast of landslide deformation trend," *Yantu Gongcheng Xuebao/Chinese Journal of Geotechnical Engineering*, vol. 32, no. 8, pp. 1291–1296, 2010.

[35] J. Liu, E. Y. Wang, Z. H. Li, and Y. K. Ma, "Multi-fractal characteristics of surface potential of coal during the fracture," *Meitan Xuebao/Journal of the China Coal Society*, vol. 38, no. 9, pp. 1616–1620, 2013.

[36] S. Hu, E. Wang, Z. Li, R. Shen, and J. Liu, "Time-varying multifractal characteristics and formation mechanism of loaded coal electromagnetic radiation," *Rock Mechanics and Rock Engineering*, vol. 47, no. 5, pp. 1821–1838, 2014.

[37] B. Kong, E. Wang, Z. Li, X. Wang, L. Chen, and X. Kong, "Nonlinear characteristics of acoustic emissions during the deformation and fracture of sandstone subjected to thermal treatment," *International Journal of Rock Mechanics and Mining Sciences.*, vol. 90, pp. 43–52, 2016.

[38] X. Kong, E. Wang, X. He, D. Li, and Q. Liu, "Time-varying multifractal of acoustic emission about coal samples subjected to uniaxial compression," *Chaos, Solitons & Fractals*, vol. 103, pp. 571–577, 2017.

[39] L. Qiu, D. Song, and X. He, "Multifractal of electromagnetic waveform and spectrum about coal rock samples subjected to uniaxial compression," *Fractals*, vol. 28, no. 4, 2020.